Electronic Supplementary Material (ESI) for Digital Discovery.
This journal is © The Royal Society of Chemistry 2024

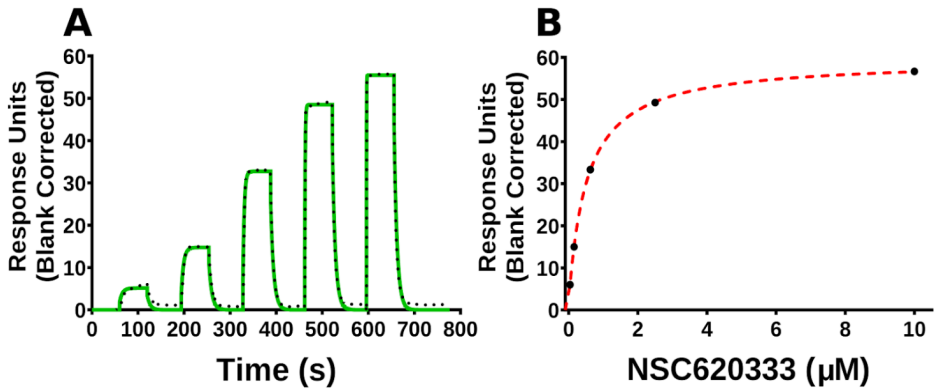

FIG. S1. **Orthogonal confirmation of NSC620333 binding to nsp14 by SPR. (A)** A representative sensorgram (solid green) is shown with the kinetic fit (black dots). From kinetic fitting, a K_D value of $427 \pm 84\,nM$, k_{on} of $3.2 \pm 0.15 \times 10^5\,M^{-1}S^{-1}$ and k_{off} of $1.3 \pm 0.2 \times 10^{-1}\,S^{-1}$ were determined. **(B)** The steady-state response (black circles) obtained from (A) is shown with the steady-state 1:1 binding model fitting (red dashed line). A steady-state K_D value of $544 \pm 22\,nM$ $(n = 3)$ was also calculated. All values are presented as mean ± standard deviation of three independent experiments $(n = 3)$.

Supplementary Information:

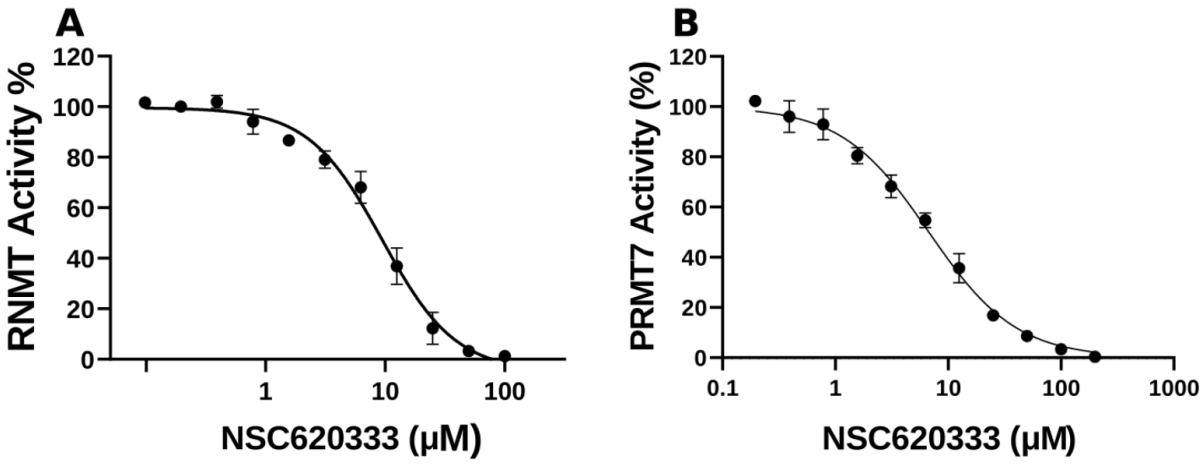

FIG. S2. **Inhibition of RNMT and PRMT7 activity by NSC620333.** (A) The IC_{50} value was determined for NSC620333 to be 8.6 ± 1.3 μM, Hill Slope: -1.5. (B) The IC_{50} value was determined for NSC620333 to be 7.0 ± 0.6 μM, Hill Slope: -1.9. The percent activity of RNMT and PRMT7 were 63 ± 7 and 32 ± 3 at 10μM of NSC62033, respectively (see Table S2). The IC_{50} value of RNMT was particularly determined because its function in human cells is the same as viral nsp14.

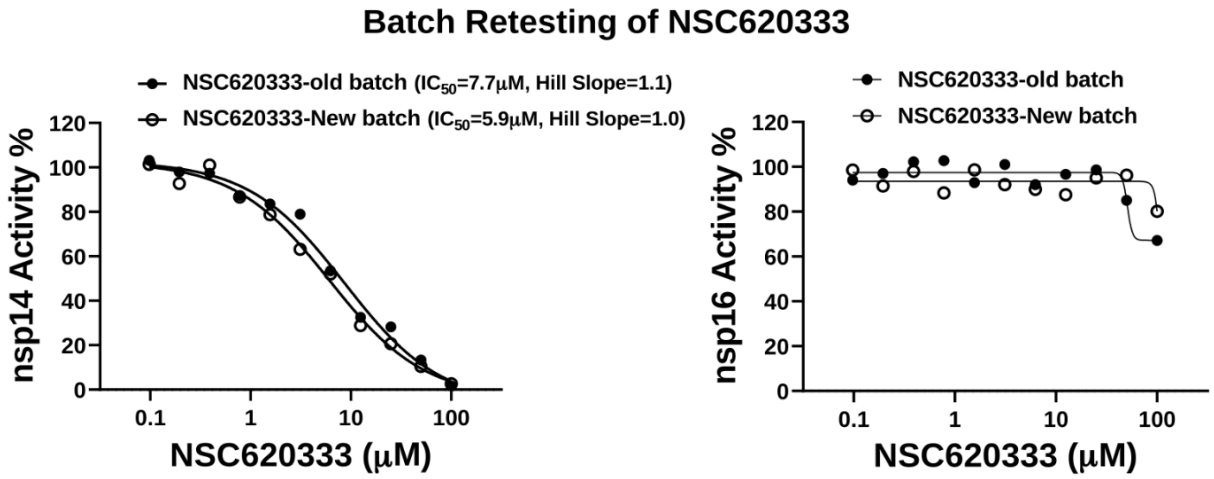

FIG. S3. **Inhibition Results from Batch Retesting of Purified NSC620333.** Outcomes of testing a custom-ordered, highly purified (>99%) sample of NSC620333. The exclusion of impurities culminated in a more pronounced inhibition of nsp14, underscoring the potency of the purified compound in the regulation of this complex.

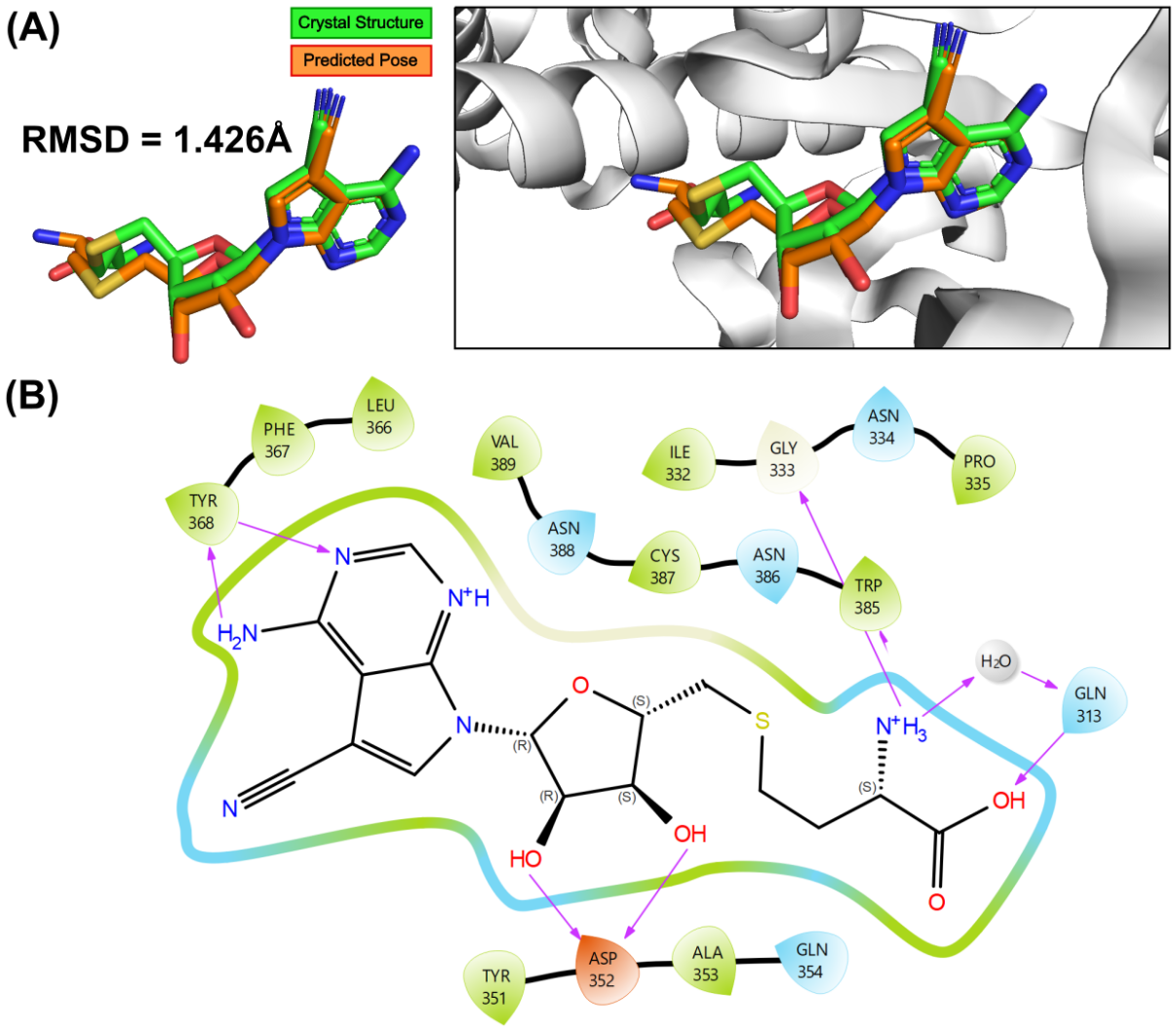

FIG. S4. **Comparative Analysis of the Crystal Structure and Predicted Docking Pose of SS148 in Complex with nsp14. (A)** Superimposition of SS148's actual crystal structure (depicted in green) and its predicted docking pose (depicted in orange), highlighting the high overlap between prediction and experiment. A Root Mean Square Deviation (RMSD) of 1.426Å is observed. **(B)** Two-Dimensional Interaction Diagram depicting the complex formation of SS148 with the nsp14 Methyltransferase (MTase), as per the actual crystal structure.

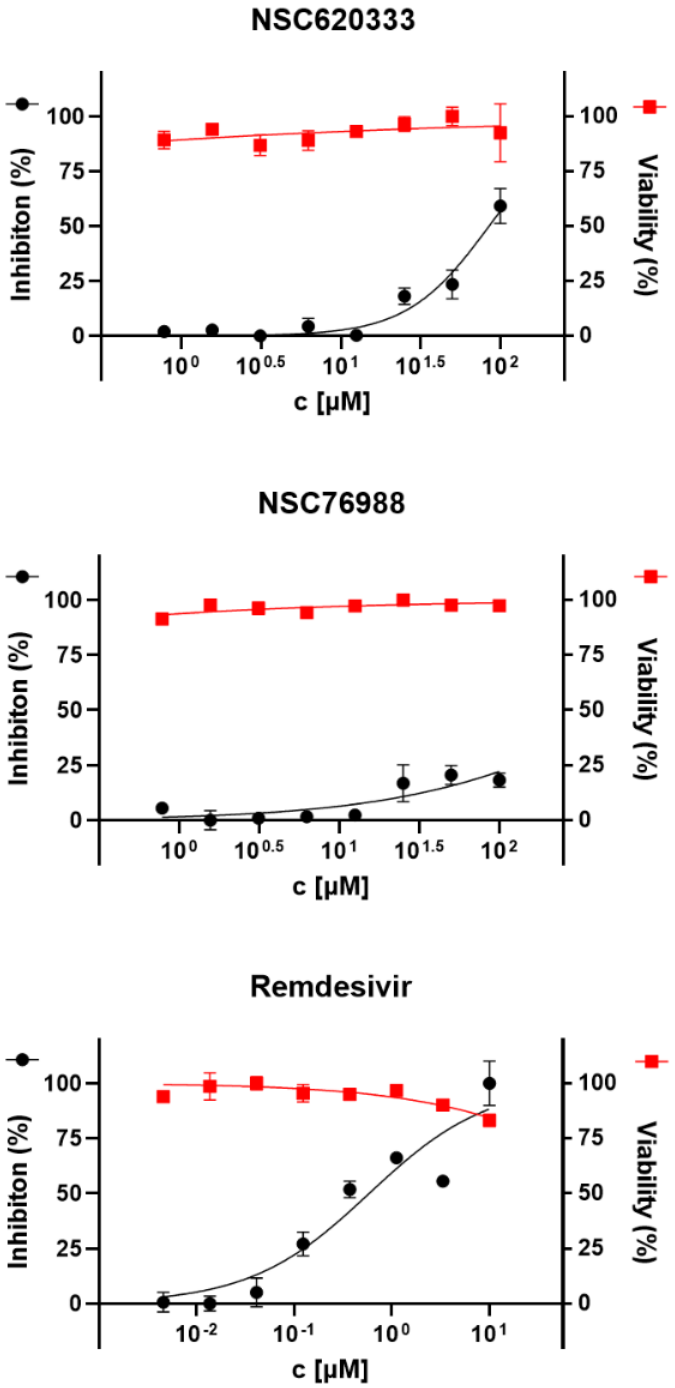

FIG. S5. **Anti-SARS-CoV-2 activity and cytotoxicity of NSC620333 and NSC76988 in Calu-3 cells.** Dose-response curve analysis of anti-SARS-CoV-2 activity (black circle) and cytotoxicity (red square) of NSC620333 and NSC76988 in Calu-3 cells. Remdesivir served as a control. All values are presented as mean ± standard deviations from experiments performed in triplicate.

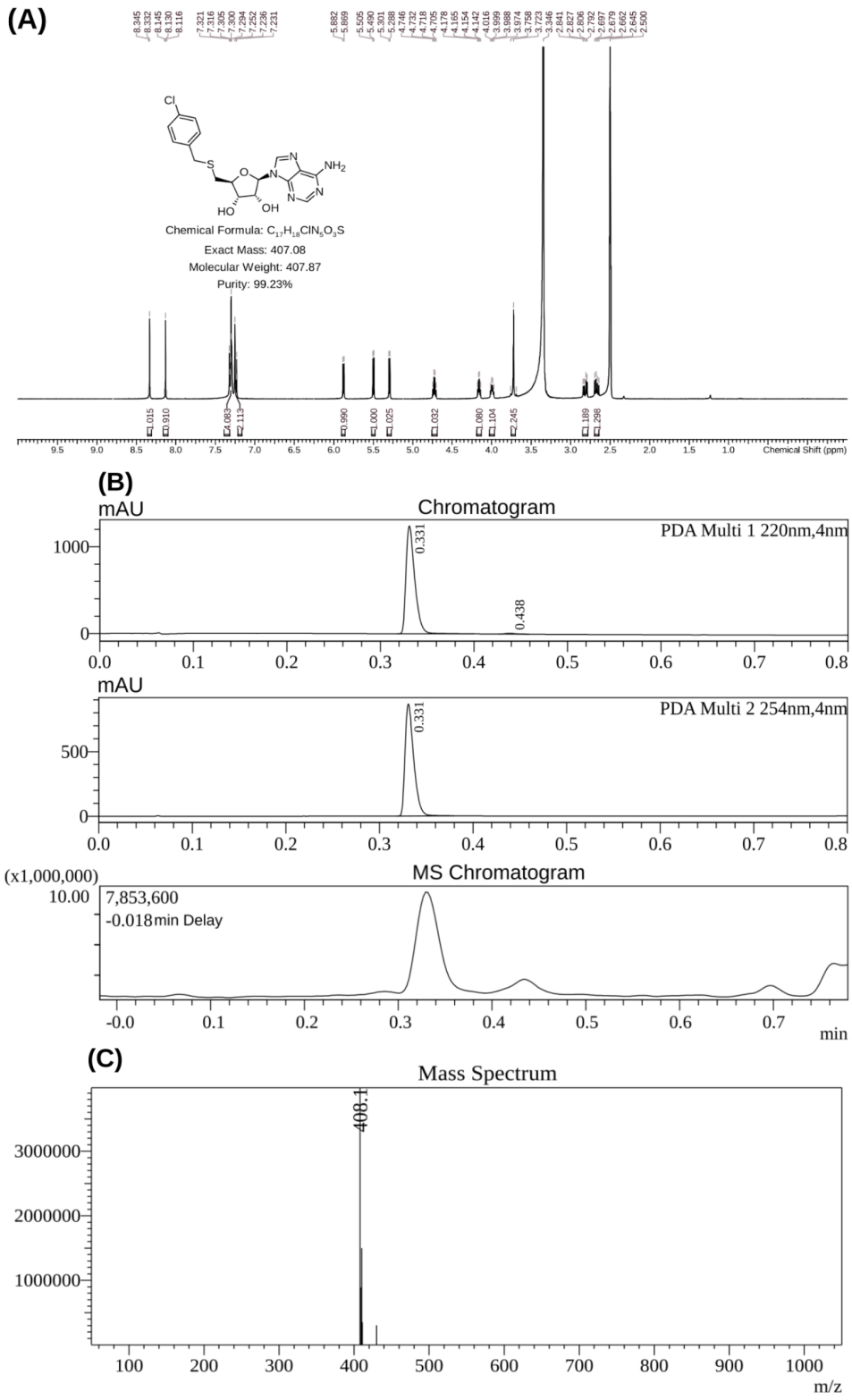

FIG. S6. Characterization data for chlorobenzothiophene 3. A. H-NMR spectrum. B. HPLC traces with both UV and MS detectors. C. High-resolution mass spectrum.

TABLE S2. **Docking and MM/GBSA Scores of Lead Compounds with nsp14.** This table presents the docking and MM/GBSA scores for 40 lead compounds in complex with nsp14, calculated using three different computational methods. The methods, in increasing order of their predictive capabilities, are Glide SP, Glide XP (both docking-based methods), and MM/GBSA. It should be noted that the MM/GBSA scores are calculated without the entropic term, potentially leading to an overestimation of binding energies. These scores are indicative of the compounds' potential interactions with nsp14 rather than direct measures of binding affinity.

Compound	Docking Score; Glide SP (kcal/mol)	Docking Score; Glide XP (kcal/mol)	MM/GBSA Score (kcal/mol)
NSC620333	-10.111	-10.728	-60.5078
NSC54251	-9.143	-10.080	-44.8260
NSC163444	-8.800	-9.520	-49.6504
NSC107661	-8.464	-9.472	-34.1128
NSC99790	-5.577	-9.373	-33.8143
NSC268226	-6.958	-8.510	-48.1415
NSC613624	-6.917	-8.477	-31.3669
NSC114010	-6.586	-8.365	-37.5531
NSC255523	-5.991	-7.907	-10.4218
NSC92432	-6.003	-7.781	-35.6097
NSC77680	-6.518	-7.769	-10.0810
NSC34443	-5.482	-7.552	-31.4914
NSC60360	-5.951	-7.539	-31.6140
NSC131119	-6.246	-7.424	-56.3134
NSC313453	-7.559	-7.261	-34.6341
NSC646375	-7.611	-7.247	-36.1022
NSC293892	-5.916	-6.851	-35.7854
NSC330685	-6.129	-6.713	-11.8248
NSC630814	-5.497	-6.385	-41.5536
NSC4348	-4.748	-6.385	-34.6630
NSC39302	-5.237	-6.365	-32.5813
NSC132916	-5.313	-6.259	-30.8526
NSC377438	-5.958	-6.242	-24.6196
NSC76988	-5.790	-6.184	-32.3499
NSC44037	-6.045	-5.975	-48.2280
NSC80136	-6.327	-5.874	-44.7396
NSC102798	-5.189	-5.831	-26.9979
NSC670682	-4.876	-5.666	-30.7842
NSC655184	-5.412	-5.619	-41.1487
NSC232469	-5.091	-5.590	-31.5946
NSC317609	-4.419	-5.521	-36.9720
NSC27605	-5.449	-5.275	-17.6311
NSC137050	-3.900	-5.217	-39.4464
NSC2269	-5.132	-5.203	-42.4074
NSC400718	-3.641	-5.061	-48.4538
NSC158437	-5.666	-4.750	-36.8949
NSC400937	-3.950	-3.729	-21.4589
NSC4624	-3.435	-3.437	-26.7526
NSC77131	-3.994	-3.330	-34.1961

TABLE S3. The percentage activity of 32 human RNA-, DNA-, and protein-MTases was assessed at a concentration of 10 µM of compound NSC62033. Data are presented as the mean ± SD from triplicate measurements.

MTases	Activity (%) at 10 µM			
	Replicate 1	Replicate 2	Replicate 3	Average
G9a	97	79	91	89 ± 9
GLP	95	105	101	100 ± 5
SUV39H1	99	91	97	96 ± 4
SUV39H2	108	96	106	103 ± 7
SUV420H1	84	97	98	93 ± 8
SUV420H2	96	104	86	96 ± 9
PRMT1	97	94	84	91 ± 6
PRMT3	75	78	85	79 ± 5
PRMT4	96	95	101	97 ± 3
PRMT5	69	64	55	63 ± 7
PRMT6	97	99	103	100 ± 3
PRMT7	35	29	32	32 ± 3
PRMT8	97	99	93	96 ± 3
PRMT9	118	118	113	117 ± 3
PRDM9	110	105	104	106 ± 3
SETDB1	104	106	100	103 ± 3
SETD2	99	103	107	103 ± 4
SETD7	85	88	87	87 ± 1
SETD8	79	90	86	85 ± 6
SMYD2	104	114	99	105 ± 8
SMYD3	101	108	91	100 ± 9
MLL1	84	87	84	85 ± 2
MLL3	44	57	53	51 ± 6
EZH2	101	90	98	96 ± 5
BCDIN3D	57	66	64	62 ± 5
DOT1L	103	90	86	93 ± 9
ASH1L	113	97	104	105 ± 8
NSD1	103	102	107	104 ± 2
NSD2	100	86	90	92 ± 7
NSD3	112	104	115	110 ± 5
nsp16/10	98	96	96	97 ± 1
RNMT	70	56	63	63 ± 7

TABLE S4. Statistics for data collection and processing, structure solution and refinement of the crystal structure of the nsp14 MTase-TELSAM/SS148 complex. Numbers in parentheses refer to the highest resolution shell. R.m.s.d., root-mean-square deviation.

Crystal	nsp14 + SS148
PDB accession code	8BWU
Space group	P 65
Cell dimensions	a, b, c (Å) 109.3 109.3 48.7 $\alpha, \beta, \gamma(^\circ)$ 90.0 90.0 120.0
Resolution range (Å)	35.78 - 2.36 (2.44 - 2.36)
No. of unique reflections	13,850 (1,383)
Completeness (%)	99.5 (98.2)
Multiplicity	19.9 (15.9)
Mean I/σ(I)	7.63 (0.54)
Wilson B factor (Å^2)	46.03
R-merge	0.3783 (3.603)
R-meas	0.3881 (3.722)
CC1/2 (%)	99.5 (42.2)
CC* (%)	99.9 (77.0)
R-work (%)	22.96 (36.39)
R-free (%)	26.43 (32.05)
CC-work (%)	94.6 (64.8)
CC-free (%)	90.9 (78.2)
R.m.s.d. bonds (Å)	0.002
R.m.s.d. angles (°)	0.42
Average B factor (Å^2)	overall 56.74 protein 57.08 ligands 41.81 solvent 45.58
Clashscore	1.42
Ramachandran (%)	favored 98.4 allowed 1.6 outliers 0.0

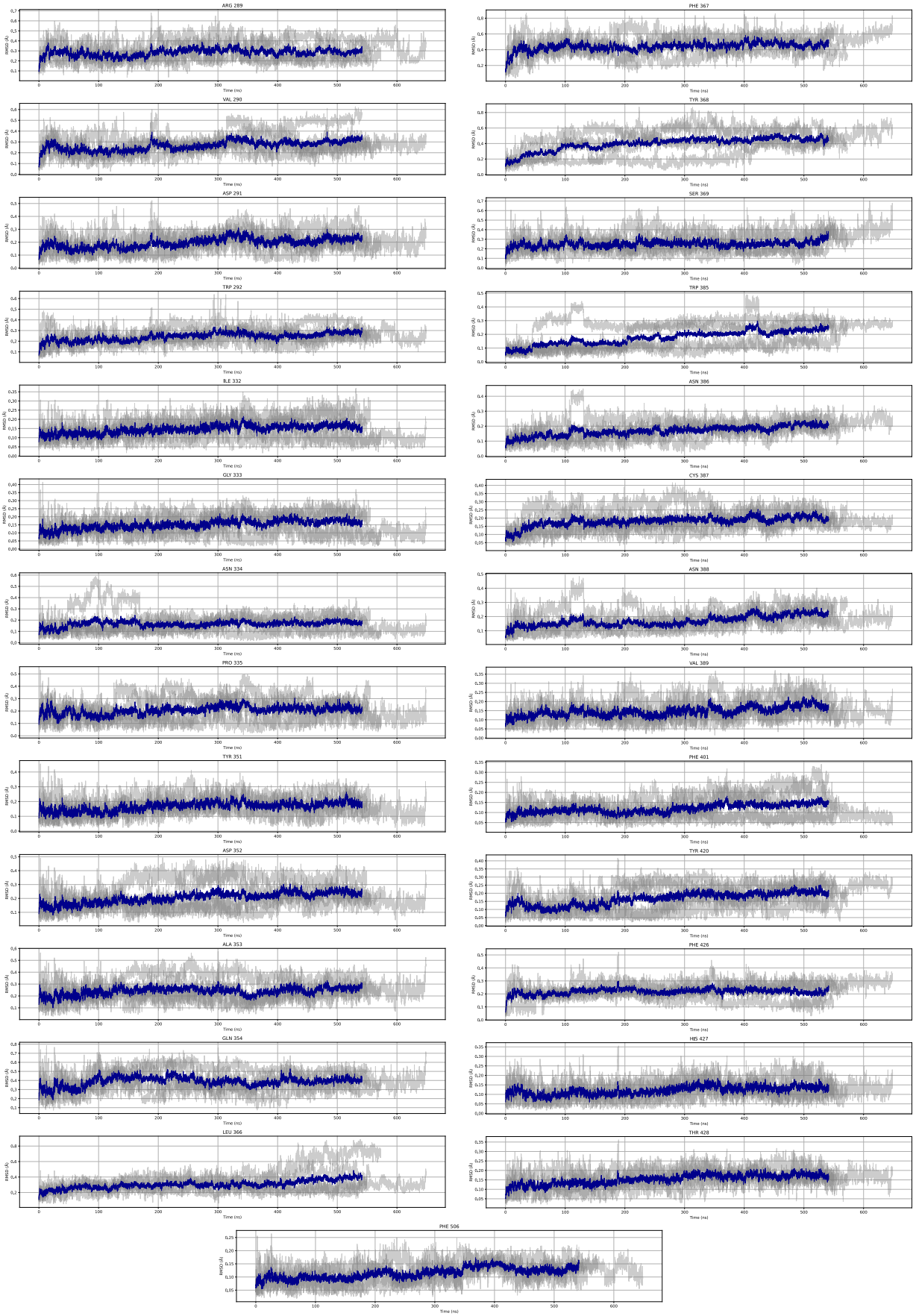

FIG. S7. **RMSD Variation of Residues in the MTase Lateral Binding Pocket Across 300.15K Simulations.** All-atom root mean square deviation (RMSD) movement of residues within the MTase lateral binding pocket during 300.15K simulations across five replicates, relative to the initial conformational structure. The RMSD values are calculated with respect to the initial static structure of the protein-ligand complex, serving as a baseline for measuring conformational changes. The individual RMSD movements for each replicate are depicted as gray lines, illustrating the diversity of conformational changes across the different simulations. The average RMSD movement, plotted in black, provides a visual summary of the typical movement exhibited by these residues in comparison to the baseline structure.

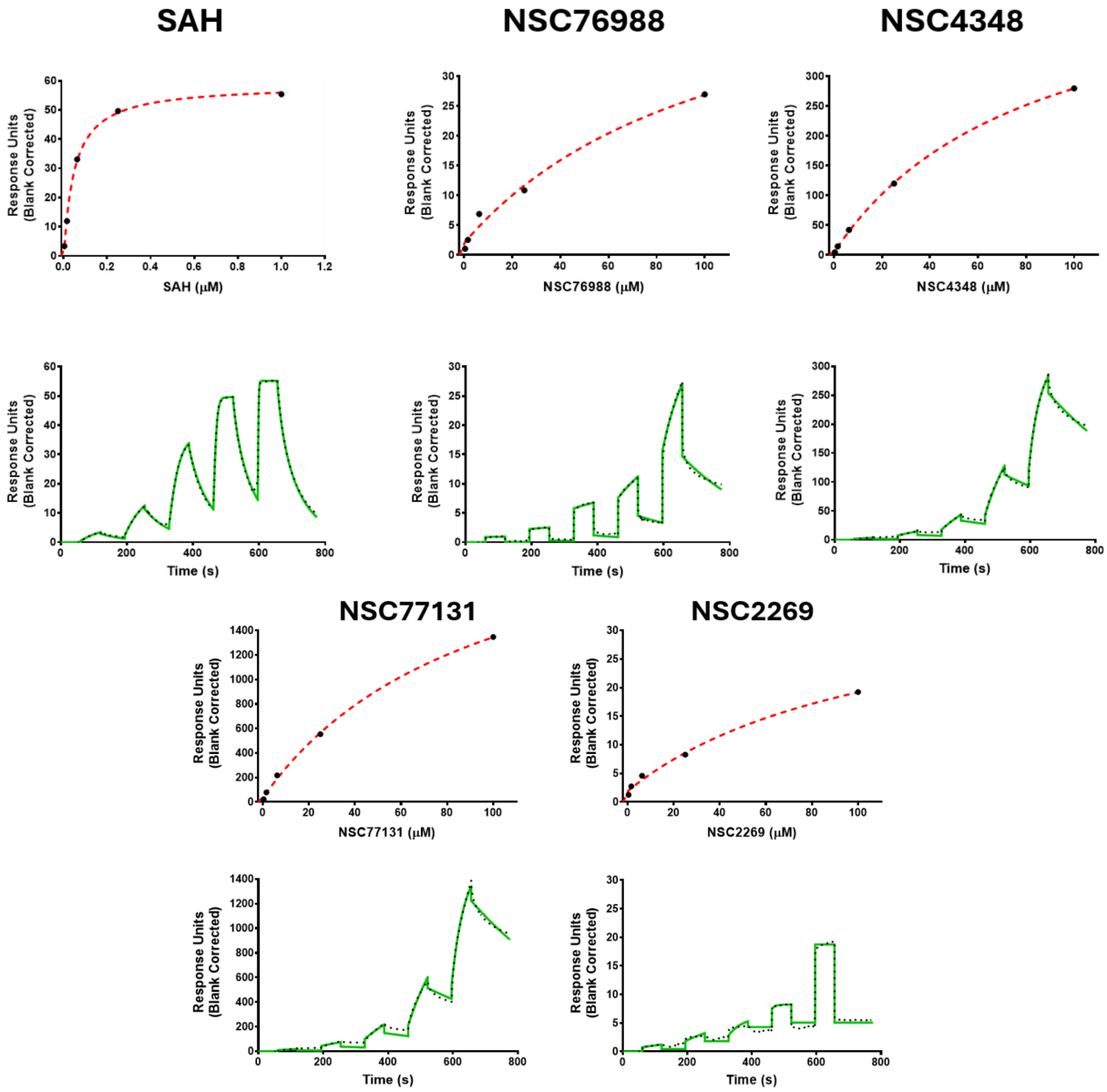

FIG. S8. **Surface Plasmon Resonance (SPR) sensorgrams and corresponding saturation curves for five compounds with previously observed MTase activity inhibition.** The plots exhibit inconclusive SPR binding results, potentially indicating experimental variability or non-specific interactions. SAH serves as a control. The upper panels show the saturation curves, while the lower panels display the sensorgrams. The response units (RU) are plotted against the compound concentrations (μM) or time (s), respectively.

TABLE S5. Compilation of NSC Numbers and their corresponding SMILES for the top 40 screened compounds.

NSC Number	Smiles
NSC39302	C1=CN=CC=C1C(=O)NNCNNC(=O)C2=CC=NC=C2
NSC4348	O[C@@H]1CO[C@](O)(CN2CCOCC2)[C@@H](O)[C@@H]1O
NSC163444	NC1=C2N=CN([C@@H]3O[C@@H]([C@@H](O)[C@H]3O)C(=O)NCC(O)=O)C2=NC=N1
NSC34443	OC[C@@H](O)[C@@H](O)[C@H](O)[C@@H](O)C1=NC2=CC=CC=C2S1
NSC107661	NC1=C2N=CN([C@@H]3OC[C@@H](O)[C@@H](O)[C@H]3O)C2=NC=N1
NSC317609	OC(=O)CCC(=O)NC[C@H]1CCC[C@@H](CNC(=O)CCC(O)=O)C1
NSC44037	NC1=NC2=NN(N=C2C(=O)N1)C1=CC=C(C=C1)C(=O)N[C@@H](CCC(O)=O)C(O)=O
NSC400718	N[C@@H](CSCCSCCSC[C@H](N)C(O)=O)C(O)=O
NSC92432	O=C(Nc1cc(O)c(cc1)C(=O)O)CCCCn1c(=O)[nH]c(=O)cc1
NSC76988	o1c2c(c(O)c(O)c(O)c2O)c(=O)cc1c1ccc(O)cc1
NSC158437	NS(=O)(=O)c1ccc(N[C@@H]2OC[C@@H](O)[C@@H](O)[C@H]2O)cc1
NSC27605	O[C@@H](=N(=O)C1=CC=NC=C1)[C@H]1OC(=O)[C@@H](O)[C@H]1O
NSC293892	CN1C2=C(C(=O)N(C1=O)C)N(C=N2)CCCNCC(C3=CC(=C(C=C3)O)CO)O
NSC60360	OC[C@H]1O[C@H](NN2C(=O)[C@H]3[C@H]4O[C@H](C=C4)[C@H]3C2=O)[C@H](O)[C@@H](O)[C@@H]1O
NSC77680	NC1=C2N=CN([C@H]3C[C@H](O)[C@@H](COP(O)(O)=O)O3)C2=NC=N1
NSC114010	N[C@@H](CC1=CC=CC=C1)C(=O)N[C@@H]1[C@@H](CO)O[C@H]([C@@H]1O)N1C=NC2=C1N=CN=C2N
NSC613624	OC[C@@H](O)[C@@H]1O[C@@H]([C@H](O)[C@H]1O)N1C=CC(=O)NC1=O
NSC54251	OCCNC1=C2N=CN([C@@H]3O[C@H](CO)[C@@H](O)[C@H]3O)C2=NC=N1
NSC313453	C[C@H](CCc1ccc2OCOc2c1)NC[C@H](O)c1ccc(O)c(c1)C(N)=O
NSC255523	O[C@@H]1[C@@H](COP(O)(O)=O)O[C@H]([C@@H]1O)N1C=NC2=C(NCC3=CC=CC=C3)N=CN=C12
NSC646375	FC(F)(F)c1cc(NC(=O)C(=O)C2C(=O)NC(=O)NC2=O)ccc1
NSC2269	O=C(c1ccc(C(=O)c2ccc(cc2)C(=O)O)cc1)c1ccc(cc1)C(=O)O
NSC620333	NC1=C2N=CN([C@@H]3O[C@H](CSCC4=CC=C(Cl)C=C4)[C@@H](O)[C@H]3O)C2=NC=N1
NSC232469	O=c1n(CCCCCCn2c(=O)[nH]c(cc2=O)C(=O)O)c(=O)cc([nH]1)C(=O)O
NSC268226	CC(C)=CCNC1=C2N=CN([C@@H]3O[C@H](COP(O)(O)=O)[C@@H](O)[C@H]3O)C2=NC=N1
NSC132916	N[C@@H](CCCNc1nc(O)c(-c2ccccc2)c(=O)[nH]1)C(O)=O
NSC670682	OC(=O)c1nc2c(nc1Nc1ccc(cc1)C(=O)O)cccc2
NSC630814	COc1cc(cc(=N(N)=S)c1O)=N1ccccc1C(O)=O
NSC137050	OC(=O)=C/C(=O)NC[C@H]1CC[C@@H](CNC(=O)=C/C(O)=O)CC1
NSC131119	N[C@@H](CCC(=O)N[C@@H](CSCc1ccc(F)cc1)C(=O)NCC(O)=O)C(O)=O
NSC99790	CN(C[C@H](O)[C@@H](O)[C@H](O)[C@H](O)[C@H](O)CO)CN1C(=O)C(=O)c2ccccc12
NSC377438	OC(=O)[C@H](Cc1ccc(O)cc1)N[C@@H](c1ccccc1)P(O)(O)=O
NSC102798	Clc1cc(S(=O)(=O)O)c(O)c(/N=N/c2c(O)cc(O)cc2)c1
NSC663881	O[C@@H]1CO[C@@](O)(COP(O)(=O)Cc2ccccc2)[C@@H](O)[C@@H]1O
NSC400937	S(=O)(=O)(O)c1ccc(/N=N/c2c3n[nH]nc3ccc2O)cc1
NSC655184	N[C@@H](CCC[C@H](N)P(O)(=O)c1ccccc1)P(O)(=O)c1ccccc1
NSC4624	S(=O)(=O)(O)c1ccc(/N=N/c2[nH]c(c(n2)C(=O)O)C(=O)O)cc1
NSC80136	O=C(NCC(=O)O)C1(NC(=O)CNC(=O)OCc2ccccc2)CCCC1
NSC77131	Oc1c(c(O)cc(O)c1)/C=C/C=C/C=C/1(=CC(=O)C=C1O)O
NSC330685	O[C@@H]1[C@@H](COP(O)(O)=O)O[C@H]([C@@H]1O)N1C=NC2=C(NCC3=CC=C(F)C=C3)N=CN=C12

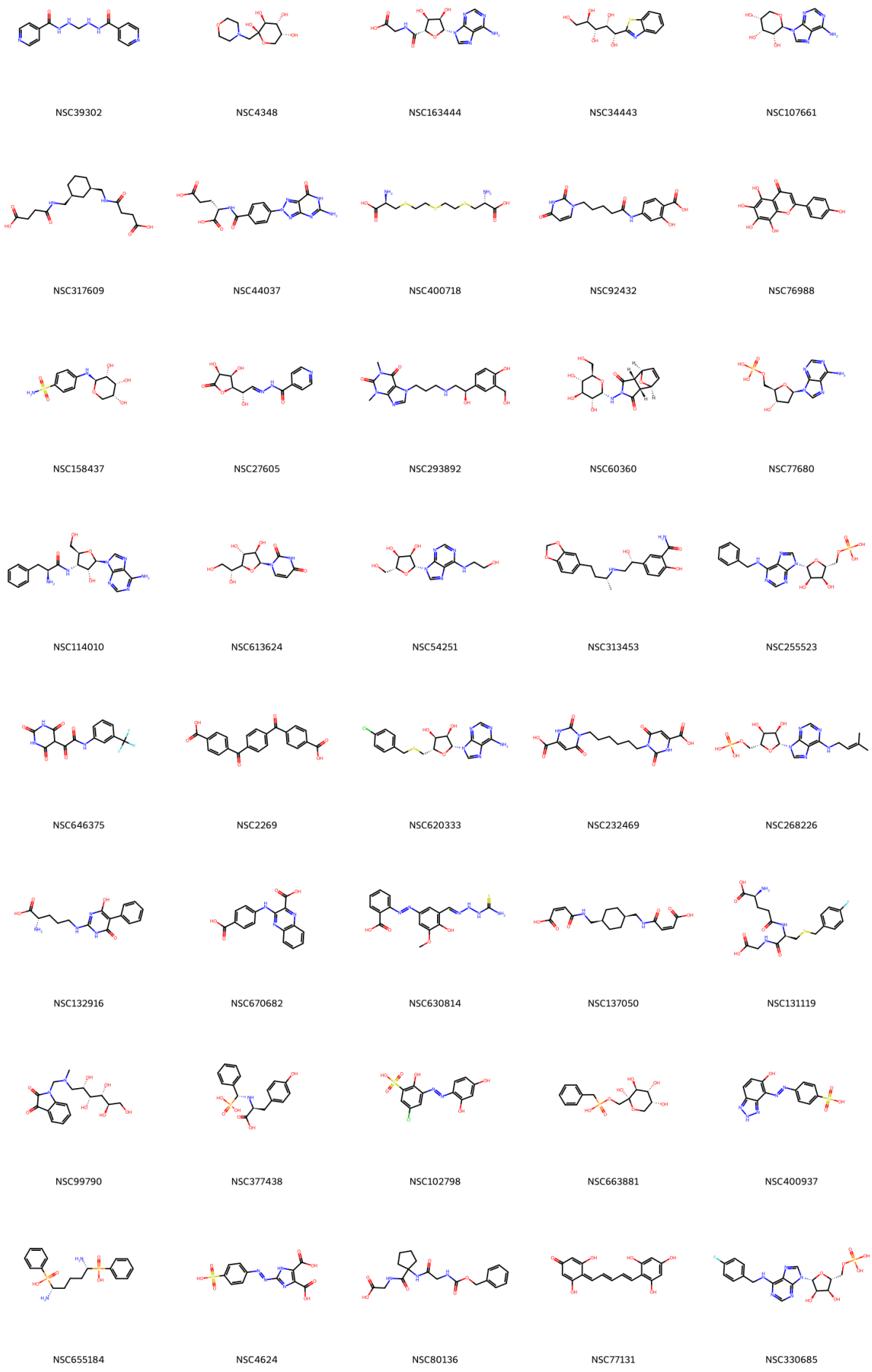

FIG. S9. Molecular structures of 40 screened compounds. Each molecule is annotated with its corresponding NSC number for easy reference.

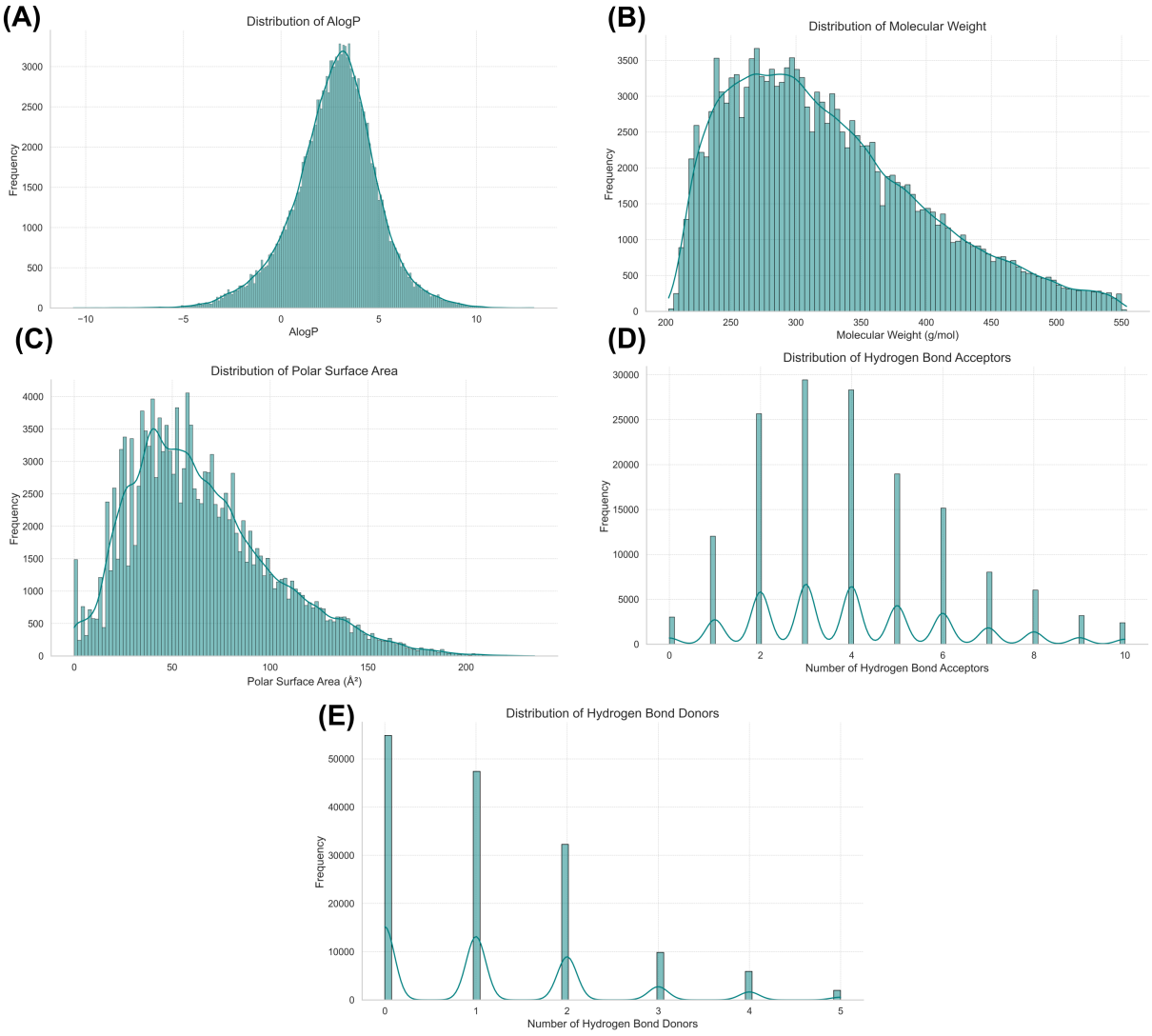

FIG. S10. Distribution of molecular descriptors in the NCI Dataset. Each panel represents the frequency distribution of a different molecular property: (A) LogP (octanol-water partition coefficient), (B) Molecular Weight, (C) Topological Polar Surface Area (TPSA), (D) Number of Hydrogen Bond Acceptors, and (E) Number of Hydrogen Bond Donors. The distributions reflect the physicochemical diversity present in the dataset and can provide insights into the drug-likeness and potential biological activity of the molecules.

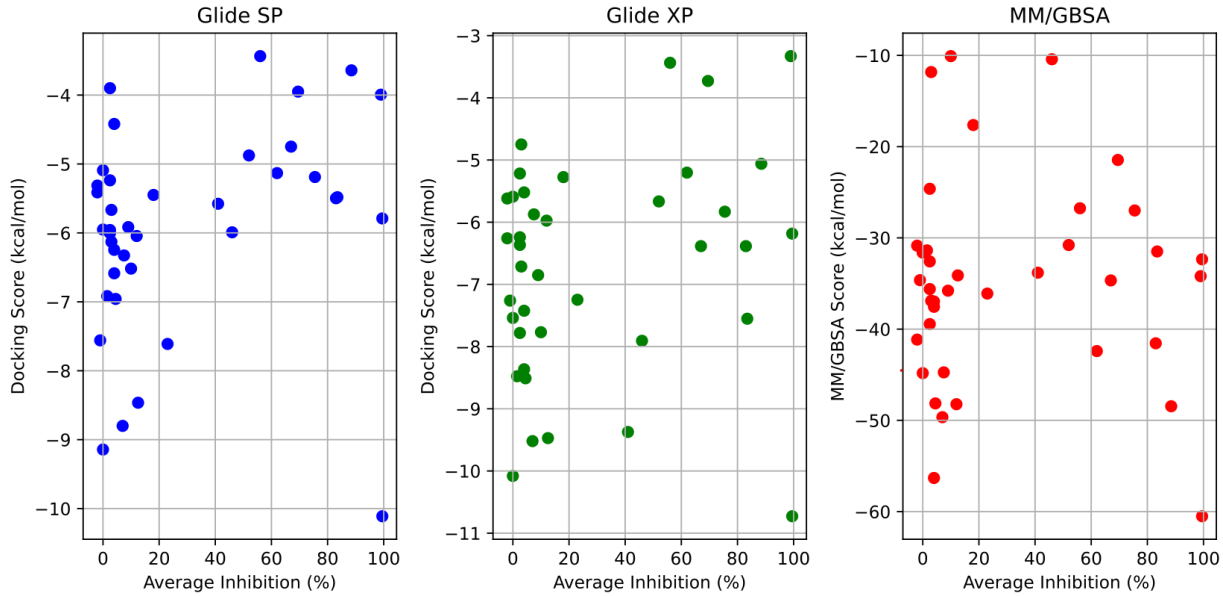

FIG. S11. Comparative Analysis of Docking Scores and Average Inhibition Percentages for Molecular Compounds Using Three Different Computational Methods: Glide SP, Glide XP, and MM/GBSA.

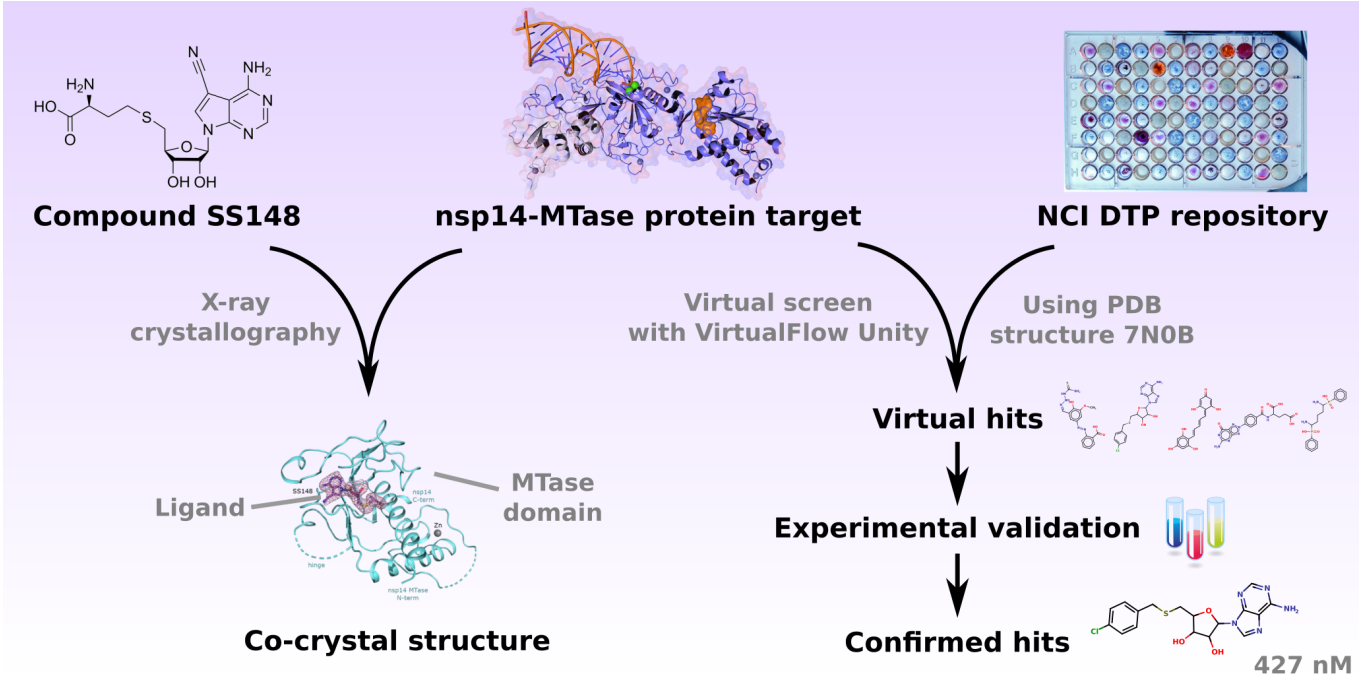

FIG. S12. TOC Image.

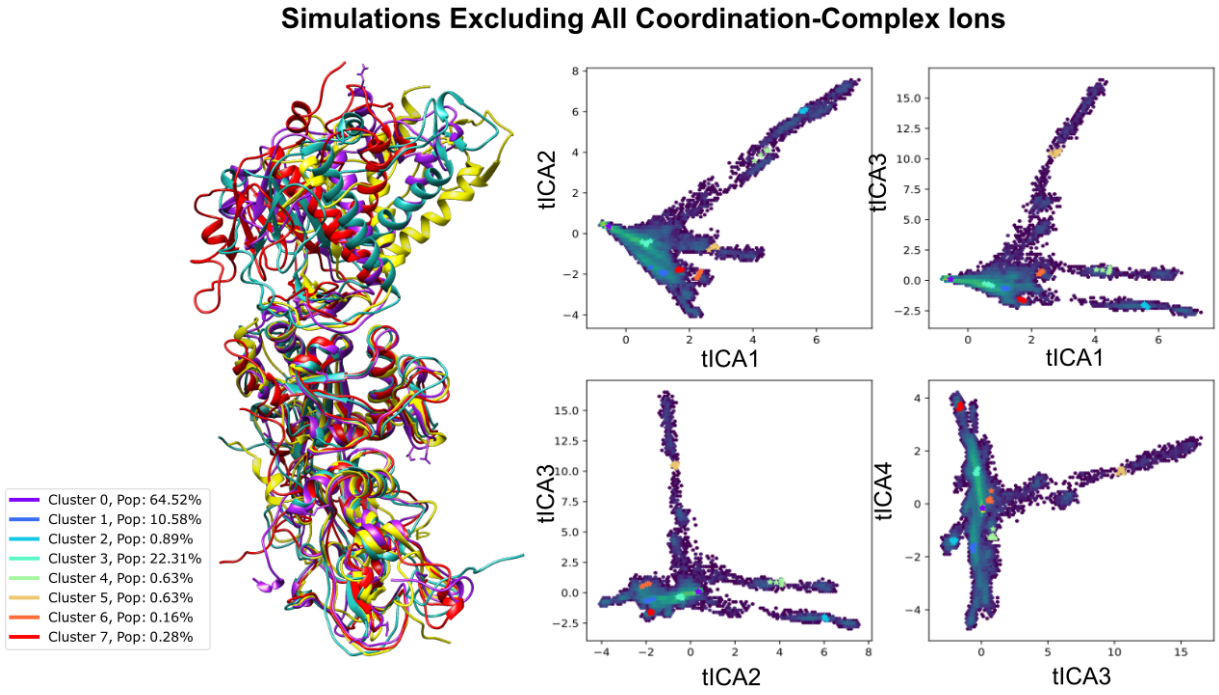

FIG. S13. **Analyzing Nsp14-nsp10 Conformational Variability through tICA Projections Influenced by Coordination Complexes.** This figure delineates the conformational differences in the nsp10-nsp14 complex under coordination-complex devoid conditions, emphasizing structures from four representative cluster centers with high variance. Trajectories were derived from independent runs between 200 ns − 1 μs, focusing on pairwise distances between alternating backbone α-carbons to determine simulation features and sampling more diverse conformations.